Earthquake and Volcano Clustering at Mono Basin (California)

D. La Marra*[,1], A. Manconi[2,3] and M. Battaglia[1]
[1]Dept of Earth Sciences, University of Rome "La Sapienza"
[2]IREA-CNR
[3] now at IRPI-CNR
*Corresponding author: P.le A. Moro 5, 00185, Roma, Italy, e-mail: lamarra.d@gmail.com

Abstract: This study investigates the feedback between fault slip and dike intrusions during the Mono-Inyo eruption sequence of ~1350 A.D. (Mono Basin, California). We perform an extensive validation of 3D finite element models against standard analytical solutions of fault dislocation in a homogeneous elastic flat half-space. The models are then applied in our analysis of the feedback mechanism between the intrusion of the Inyo dike and slip along the Hartley Springs fault.

Keywords: Mono Basin, structural-magmatic interactions, earthquake, fault, dike.

1. Introduction

Mono Basin is a post-Miocene northward trending graben situated east of the Sierra Nevada, extending from the northern edge of Long Valley Caldera to Body Hills, north of Mono Lake. From a hydrographic perspective, the Mono Basin is defined by all streams that drain into Mono Lake.

The Mono-Inyo Craters volcanic chain forms a northward trending line of volcanic vents extending 45 km from the west moat of the caldera to Mono Lake. Volcanism and tectonic deformation (~ 0.5 m/kyr) have been synchronous, and their manifestations are interrelated *(Christensen et al., 1969)*. There has been a tendency for the Mono chain to propagate both northward and southward in the late Holocene. This tendency continued with southward propagation of the Inyo dike, whose eruptions (in the mid-14th century) followed the North Mono eruption by at most a few years *(*Figure 1; *Bursik and Sieh, 1989; Hildreth, 2004)*. Stratigraphic data suggest that during the North Mono-Inyo eruption sequence of ~1350 A.D. a series of strong earthquakes (5.5<Mw<6.5) occurred near the end of the North Mono explosive phases and the beginning of the Inyo explosive phases. The temporal proximity of these events suggests the possibility of a causal relationship. Geological and geomorphic features of the Hartley Springs Fault (HSF) are consistent with rupture of the fault during the eruption sequence *(Bursik et al., 2003)*.

The use of the Finite Element Method (FEM) may play an important role in the study of the feedback between the dike intrusion and the fault slip. In this context, we investigate how the local stress field changes because of the Inyo dike (ID) intrusion, how this can facilitate slip along the HSF, or how the slip may help the propagation of the ID to the surface.

In the following sections, we will focus on the validation of the FE model against analytical solutions for a rectangular dislocation in a homogeneous, elastic flat half-space. We will also present a number of preliminary results of our geodynamic model.

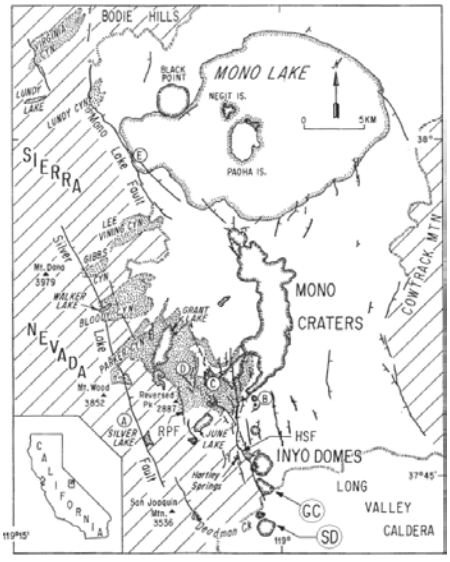

Figure 1. The Mono Basin area: HSF is the Hartley Springs fault, extending from the northern rim of Long Valley caldera to the June Lake. HSF intercepts the Inyo craters that are trending approximately N-S *(*after *Bursik and Sieh, 1989).*

2. FEM Model Implementation

The 3D FEM model is implemented using the Structural Mechanics module of COMSOL. The crust is modeled as a homogeneous elastic flat medium (width and length 200 km, depth 30 km), divided in cylindrical sub-domains with increasing radii to achieve a gradual refining of the mesh toward the centre of the domain (Figure 2).

The elastic constants of the medium are estimated from typical values of seismic velocities for granite and using appropriate conversion relations *(Brocher, 2005)*. This gives a Poisson's ratio ν equal to 0.25, a Young's module E equal to 67 GPa, a shear modulus G of 27 GPa and a rock density ρ equal to 2670 Kg/m^3. The boundary conditions are set as free surface at the top, and roller at the bottom and sides of the model.

We simulate the HSF and the ID as mechanical discontinuities. The HSF is approximated by a vertical plane 9.5 km-long and 10 km deep with contact pairs between the fault subdomain (Figure 2). The top edge of the fault is 10 m below the free surface to avoid numerical stability problems. The plane surfaces that do not belong to the fault subdomain are treated as identity pairs.

To take into account the friction interaction, we set the static friction coefficient equal to 0.5. We set an initial contact pressure and friction force (x, y, z direction) equal to zero, a contact normal penalty factors equal to E/h where h is the mean mesh size and a contact surface offset equal to -10. These parameters have been calibrated to facilitate the convergence of the model.

The dike is simulated by a rectangular cavity 10 km-long, 10 m-wide, and 7 km-deep, reaching to within 300 m from the surface (Figure 2). A normal opening load is applied to the vertical sides, while the shorter sides are free. The mesh size is set to *extra fine* in the free mesh parameters (Figure 2). In particular:

- in subdomain (4) and (5), and in the mutual boundaries surface, the maximum element size is respectively 900 and 500 with an element growth rate of 1.3;
- in subdomain (3), the same parameters are 2000 and 1.3;
- in subdomain (2), 4000 and 1.4;
- the rectangular subdomain (1) is set with a maximum element size of 6000 and an element grow rate of 1.4;
- the vertical mesh for the fault and dike has a maximum element size of 300 and an element growth rate of 1.15.

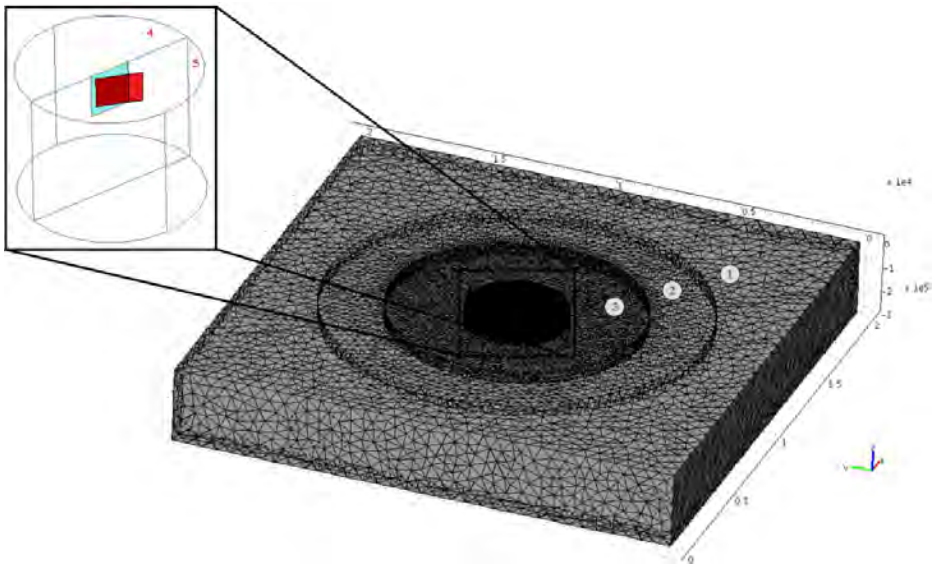

Figure 2. 3D geodynamic model: geometry and mesh. The light-blue surface (left) is the master contact plane of HSF, the red surface (left) is the Inyo dike. The numbers label the internal cylinder subdomains.

To solve the model, we set the analysis type to static and choose PARDISO as the linear system solver. For the non linear setting, we choose a relative tolerance of 1E-06 and a maximum number of iterations of 200.

3. FE Model Validation

We validate our FEM model against the *Okada (1992)* analytical solutions for a rectangular dislocation in a homogeneous elastic flat half-space. *Okada (1992)*'s model is usually employed in simulations of fault dislocations that may represent both earthquakes and dike intrusions. We carried out several tests that allowed us to determine the optimal parameters and boundary conditions necessary to reproduce the analytical solutions. In particular, the correct choice of boundary conditions has been critical to replicate the analytical solutions by *Okada (1992)*. In Figure 3 and Figure 4, we compare numerical and analytical results along several profiles parallel to the x-direction for different depths and distances from the rectangular dislocation source.

3.1 Fault Validation

We study possible configurations of the HSF by considering both vertical (90° dip) and sub-vertical (60° dip) shear and normal dislocations.

We set the contact planes as master-master with a total prescribed displacement of 1 m in the direction of slip (right-lateral strike slip) and 0 m in the tangential direction. The fault plane normal to the slip was left free to move. These boundary conditions allow the implementation of a dislocation source consistent with the analytical solution by *Okada (1992)*. The results for the vertical and inclined strike-slip dislocation and the vertical tensile opening show a good agreement between the numerical and analytical models (Figure 3). Some anomalies are present at the maximum and minimum value of FEM results and near the depth bottom of model. We believe that these differences are strongly influenced by the mesh resolution. The validation of the sub-vertical dip slip is more difficult and is still under investigation.

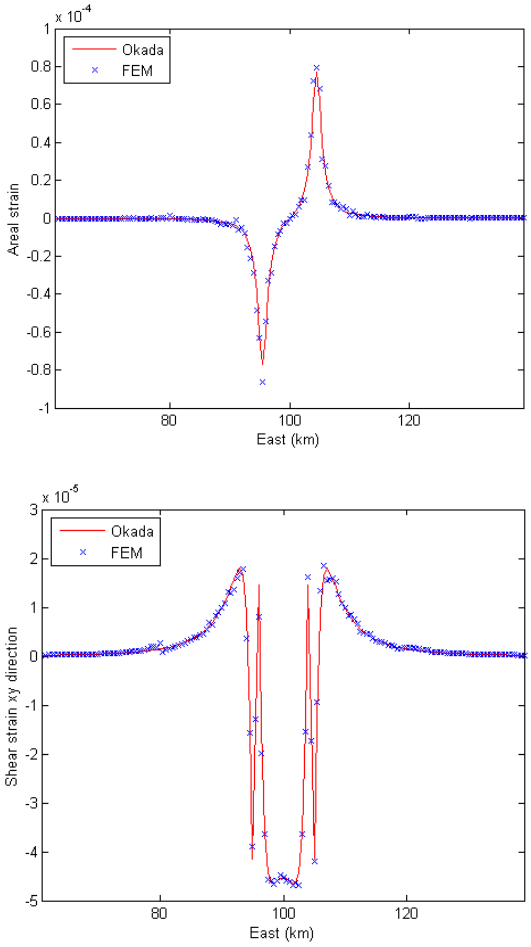

Figure 3. Vertical fault validation. Line cross-section plots: areal strain, and shear strain 1 km from the fault plane at the surface.

3.2 Dike Validation

We applied two different procedures to draw the geometry of the ID: (a) a rectangular contact plane; (b) a rectangular cavity (see Section 2 for parameters). The dike opening is simulated by imposing a total normal prescribed displacement of 1 m to the vertical sides. The other directions of slip are left free to move. Both dike models reproduce well the analytical solutions for a tensile dislocation but the best results are achieved with the model (b), see Figure 4.

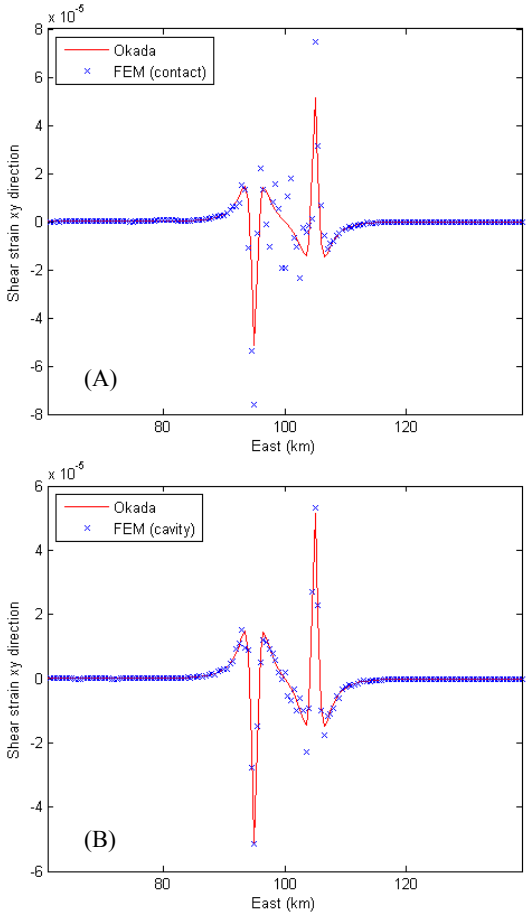

Figure 4. Line cross-section plots: shear strain at the surface along a profile 1 km from the source; (a) dike as contact; (b) dike as cavity.

4. Mono Basin Geodynamic Model

We use a three steps procedure to investigate the feedback mechanism between the ID and the HSF. First, we study the Coulomb stress change for the ID tensile dislocation setting the HSF as a passive receiver. This allows us to determine the condition of rupture along the fault plane. Second, we analyze the right-lateral displacement along the HSF fault, and the local stress distribution between the HSF and ID. Finally, we compute the local stress change caused by a shear dislocation consistent with the magnitude of the earthquake of ~1350 A.D.

The normal driving pressure values for the dike are extrapolated from the model of *Reches and Fink (1988)*:

$$\left[P_d\right]_z = P_m - \sigma_t \qquad (1)$$

where $\left[P_d\right]_z$ is the driving pressure opening applied to normal direction of the dike vertical sides, σ_t is the tectonic stress upper 10 km of the crust in the Inyo area. P_m is the dike magma pressure

$$\left[P_m\right]_z = \left(P_h - P_{vis}\right) + P_v - P_f - P_e \qquad (2)$$

and depends from five components: the hydrostatic pressure in the magma, P_h, the pressure drop due to viscous resistance, P_{vis}, the volatile overpressure, P_v, the fracture strength, P_f, and the elastic resistance, P_e *(Reches and Fink, 1988)*. This last component is defined as a difference between the internal hydrostatic pressure in the crack and the external hydrostatic pressure in the host rock

$$P_e = \frac{W}{L}\frac{\mu}{1-\nu} \qquad (3)$$

Since the combination of $P_v - P_f - P_e = P_{con}$ is practically constant *(Reches and Fink 1988)*, an increase of the elastic resistance P_e does not involve a change in the driving pressure (Figure 5).

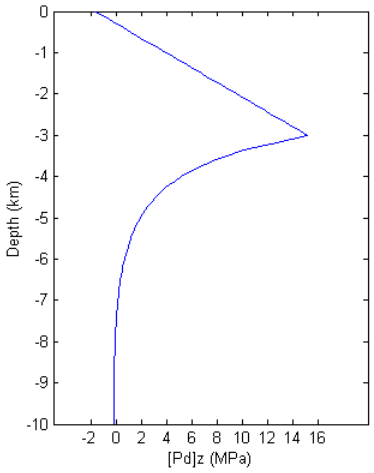

Figure 5. Driving pressure $\left[P_d\right]_z$ applied as tensile component to the vertical sides of the Inyo Dike.

The Coulomb failure criterion, allows us to identify the areas that might encouraged or discouraged to fail in a future event. The Coulomb failure criterion can be written as *(Harris, 1998)*

$$\Delta CFS = \Delta\tau + \mu'\Delta\sigma \qquad (4)$$

If we assume that the soil is dry (note that the study area is desert-like) then the maximum Coulomb stress change for a right-lateral slip along the fault plane due to the dike opening is 5.7 MPa (*King et al., 1994;* Figure 6). The positive change of Coulomb stress highlights that only the region near the south tip of HSF is encouraged to slip right-laterally. For this configuration, the strike-slip movements triggered by the ID show a prevalent left-lateral component. This result is clearly not consistent with the geological data. Indeed, the north-northwest trending faults in Mono Basin seem to accommodate the tectonic strain with oblique and right-lateral slip *(Bursik and Sieh, 1989)*. Furthermore, the limited right-lateral slip along the HSF simulated by our model would not reproduce the earthquakes occurred ~1350 A.D. To solve this issue additional simulations varying the geometry and dimensions, as well as the orientation, of the ID will be necessary.

To investigate the feedback mechanism between ID and HSF, we analyze the principal stress change caused by a shear dislocation along the fault. Following *Gudmundsson (2006)*, we assume that dykes are mostly extension fractures that intrude following the direction of the maximum principal compressive stress σ_1 and open perpendicular to the minimum compressive (maximum tensile) principal stress σ_3. Dike intrusions depend on the distribution of maximum tensile stress, and a local increase of the maximum tensile stress can favor the dike propagation to the surface.

Starting by the previous results of the previous model, we set the fault as master-master contact pairs with a total prescribed strike-slip displacement of 1 m to simulate an earthquake of magnitude Mw ~6.24.

Figure 7 show stress changes due to the dike opening or the slip along the fault. The results show a local increase of maximum tensile stress in the region between the dike and the fault. This increase in the tensile stress (or reduction in the compressive stress) may favor the propagation of a dike toward the surface.

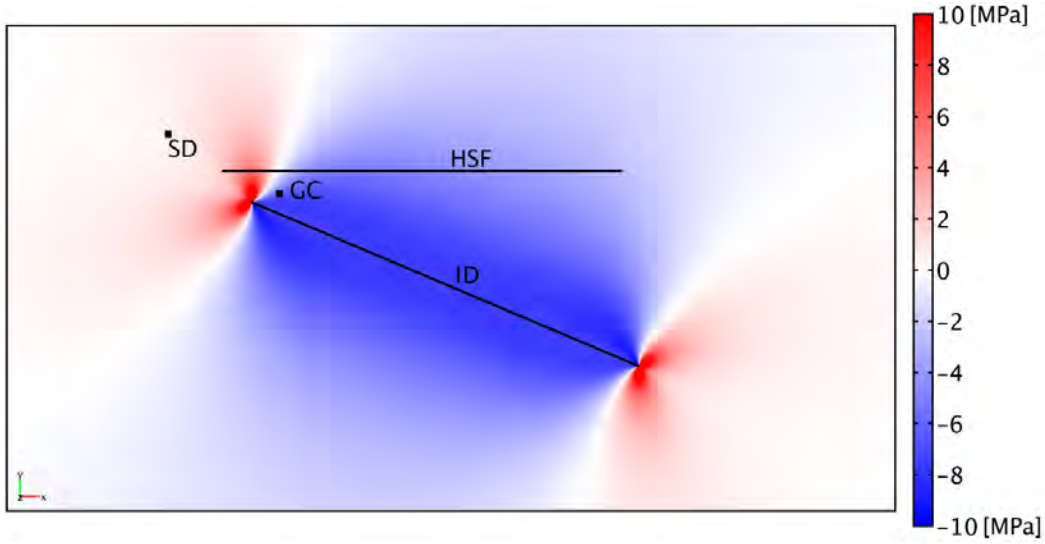

Figure 6. Coulomb stress change triggered by the opening of the ID along a plane oriented as the HSF. The stress would encourage left-lateral slip along the fault. The plot shows the maximum Coulomb stress on the HSF at a depth of 2.5 km. Squares indicate the locations of the Glass Creek (GC) and South Deadman (SD) flow.

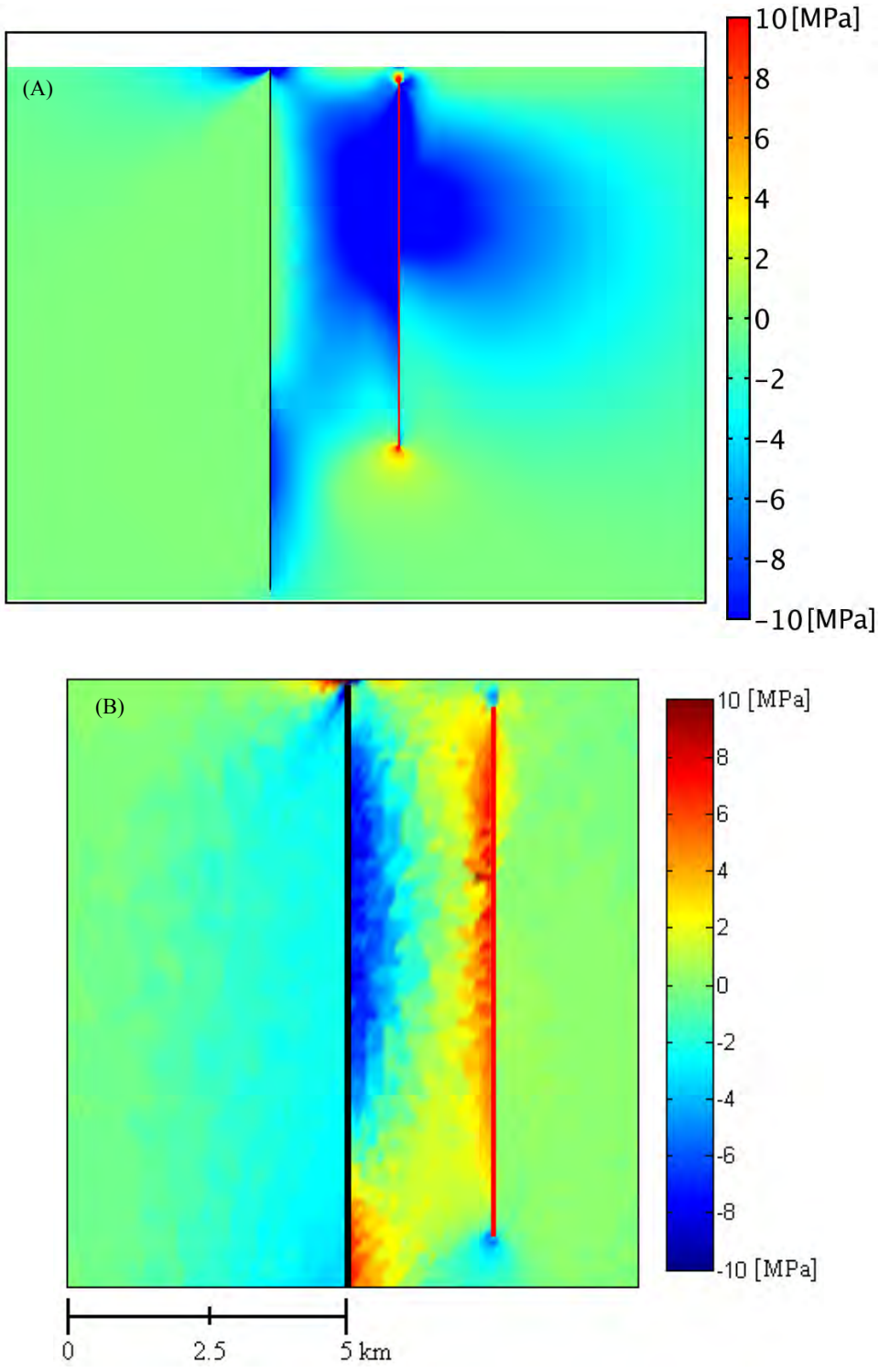

Figure 7. Plots of maximum tensile stress: (A) maximum tensile stress caused by the dike opening for static condition of HSF; (B) stress change triggered by right-lateral strike-slip along the HSF. The black line indicates the HSF and the red line indicates the Inyo dike.

5. Summary and Conclusions

In this paper we use FEM models to simulate the feedback mechanism between the intrusion of the ID and slip along HSF during the North Mono-Inyo eruption sequence of ~1350 A.D.

We first compared our model against standard models of the fault dislocation problem. We found good agreement between the stress and the strain computed analytically and those simulated numerically.

Our preliminary results indicate that the opening of the ID would favor left-lateral strike slip motion along the HSF with right lateral slip possible only at the tip of the HSF. This scenario is not consistent with the geological evidences from the earthquakes of ~1350 A.D.

On the other hand, the maximum tensile principal stress change due to strike-slip along the HSF induces an increase of the local tensile stresses, facilitating the opening the ID and the possibility of intrusion toward the surface.

Future studies will investigate the influence of mechanical heterogeneities, topography and different orientations and geometries of the Inyo dike.

6. References

1. Brocher T. M., Empirical Relations between Elastic Wavespeeds and Density in the Earth's Crust, Bull. *Seismol. Soc. Am.*, **95 (6)**, 2081-2092 (2005)

2. Bursik M., Renshaw C., McCalpin J. and Berry M., A volcanotectonic cascade: Activation of range front faulting and eruptions by dike intrusion, Mono Basin-Long Valley Caldera, California, *J. of Geophy. Res.*, **108 (B8)**, 2393-2407 (2003)

3. Bursik M. and Sieh K., Range Front Faulting and Volcanism in the Mono Basin, Eastern California, *J. of Geophy. Res.*, **94 (B11)**, 15,587-15,609 (1989)

4. Christensen M. N., Gilbert C. M., Lajoie K. R. and Al-Rawi Y., Geological-Geophysical Interpretation of Mono Basin, California-Nevada, *J. of Geophy. Res.*, **74 (22)**, 5221-5239 (1969)

5. Gudmundsson A., How local stresses control magma-chamber ruptures, dyke injections, and eruptions in composite volcanoes, *Earth-Science Reviews*, **79**, 1-31 (2006)

6. Harris R. A., Introduction to special section: Stress triggers, stress shadows, and implications for seismic hazard, *J. of Geophy. Res.*, **103 (B10)**, 24,347-24,358 (1998)

7. Hildreth W., Volcanological perspectives on Long Valley, Mammoth Mountain, and Mono Craters: several contiguous but discrete systems, *J. of Volcanology and Geothermal Research*, **136**, 169-198 (2004)

8. King G. C. P., Stein R. S. and Lin J., Static Stress Changes and the Triggering of Earthquakes, *Bull. Seismol. Soc. Am*, **84 (3)**, 935-953 (1994)

9. Okada Y., Internal Deformation Due to Shear and Tensile Faults in a Half-Space, *Bull. Seismol. Soc. Am.*, **82 (2)**, 1018-1040 (1992)

10. Reches Z. and Fink J., The Mechanism of Intrusion of the Inyo Dike, Long Valley Caldera, California, *J. of Geophy. Res.*, **93 (B5)**, 4321-4334 (1988)

7. Acknowledgements

This project was supported by a grant from the MIUR program "Rientro dei Cervelli".